Inorganic Chemistry

Article

pubs.acs.org/IC

Magnetic Relaxation of 1D Coordination Polymers $(X)_2[Mn(acacen)Fe(CN)_6]$, X = Ph_4P^+, Et_4N^+

Michał Rams,*[,†] Eugenia V. Peresypkina,[‡] Vladimir S. Mironov,[§] Wolfgang Wernsdorfer,[∥] and Kira E. Vostrikova*[,‡,⊥]

[†]Institute of Physics, Jagiellonian University, Reymonta 4, 30-059 Kraków, Poland

[‡]Nikolaev Institute of Inorganic Chemistry, 3 Lavrentiev avenue, 630090 Novosibirsk, Russia

[§]A. V. Schubnikov Institute of Crystallography, RAS, 59 Lenin avenue, 119333 Moscow, Russia

[∥]Institut Néel, CNRS, 25 rue des Martyrs, F-38042 Grenoble, Cedex 9, France

[⊥]LMI, Université Claude Bernard Lyon 1, 69622 Villeurbanne Cedex, France

Supporting Information

ABSTRACT: Substitution of the organic cation X in the 1D polymer, $(X)_2[Mn(acacen)Fe(CN)_6]$, leads to an essential change in magnetic behavior. Due to the presence of more voluminous Ph_4P^+ cations, the polyanion has a more geometrically distorted chain skeleton and, as a consequence, enhanced single chain magnet (SCM) characteristics compared to those for Et_4N^+. The Arrhenius relaxation energy barriers, the exchange interaction constant and the zero-field splitting anisotropy of Mn^{III} are determined from the analysis of magnetic measurements. The discussion is supported with ligand field calculations for $[Fe(CN)_6]^{3-}$ that unveils the significant anisotropy of Fe magnetic moments.

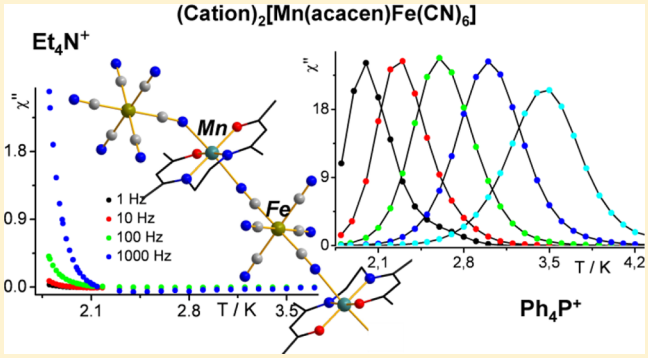

INTRODUCTION

Molecular magnetism is a quickly extending field of research. Its central subject is the design and study of magnetic molecular materials with variable properties appropriate for future types of electronic and magnetic devices.[1] Compared to conventional magnets, molecular magnetic materials possess the major benefits: they are lightweight, are soluble, and display multifunctionality.[2] During the last dozen years significant attention was devoted to the design and investigation of low-dimensional (0D and 1D) polynuclear compounds exhibiting slow relaxation of magnetization and magnetic hysteresis at low temperatures,[3] because they may have possible applications in information technologies such as molecular electronics, molecular spintronics, and quantum computing.[4] The discovery of one-dimensional (1D) polymeric metal complex in 2001,[5] demonstrating slow magnetic dynamics, inspired intense research activity in this new field of molecular magnetism, which is now known as single chain-magnets, SCMs.[6−8]

SCM behavior may be observed in crystals built of coordination polymers in which the intrachain spin coupling is stronger than the interchain interaction by several orders of magnitude. Despite the lack of long-range magnetic order at a finite temperature, SCMs may exhibit a remanent magnetization due to slow magnetic relaxation below a blocking temperature (T_b). As shown by Glauber in 1963, the relaxation time of magnetic susceptibility for the infinite chain of ferromagnetically coupled Ising spins follows the Arrhenius law with an activation energy barrier.[9] This barrier is equal to the energy required to create two very narrow domain walls that can move leading to relaxation of magnetization. In a more general model, chains of spins with uniaxial single-ion anisotropy and Heisenberg exchange interaction are considered. If the energy of the exchange interaction is stronger than the anisotropy energy, the domain wall is no longer narrow, but the Arrhenius law still governs magnetic relaxation. To increase the activation energy barrier in such a SCM, it is beneficial to augment the magnetic anisotropy, as well as the exchange interaction between spins within the chains.[7] In real systems, when the defects of the crystal break chains into finite segments, the relaxation process is also due to single domain wall migration through the chain that essentially modifies the relaxation time compared to those for the infinite system.[10]

Cyano-bridged metal assemblies have provided a large number of materials with SMM[11] and SCM behavior.[12] Among these materials, several based on hexacyanoferrate(III) ion heterometallic SMM clusters[13] and magnetic chains[14−16] were prepared and magnetically characterized. The octahedral $[Fe(CN)_6]^{3-}$ anion represents an important orbitally degenerate magnetic building block with unquenched orbital momentum and its incorporation in SCMs and SMMs can potentially increase their magnetic anisotropy.

Received: June 6, 2014
Published: September 15, 2014

Table 1. Crystal Data, Data Collection, and Structure Refinement Parameters for 2

Crystal Data	
chemical formula	$(C_{18}H_{18}FeMnN_8O_2)\cdot 2(C_{24}H_{20}P)\cdot 0.5(C_2H_5OH)\cdot C_3H_7OH$
M_r	1251.06
crystal system, space group	triclinic, $P\bar{1}$
temperature (K)	100.0(2)
a, b, c (Å)	13.3007(4), 15.2241(4), 18.5888(5)
α, β, γ (deg)	94.085(1), 110.098(1), 114.038(1)
V (Å^3)	3128.88(15)
Z	2
$F(000)$	1308
radiation type	Mo Kα
μ (mm^{-1})	0.54
crystal size (mm)	0.47 × 0.17 × 0.11
Data Collection	
diffractometer	Apex DUO diffractometer
absorption correction	empirical, based on intensities[20]
T_{min}, T_{max}	0.697, 0.746
no. of measured, independent and observed $[I > 2\sigma(I)]$ reflections	22202, 14307, 10653
R_{int}	0.030
$(\sin\theta/\lambda)_{max}$ (Å^{-1})	0.650
range of h, k, l	$h = -17 \rightarrow 17$, $k = -18 \rightarrow 19$, $l = -24 \rightarrow 16$
Refinement	
$R[F^2 > 2\sigma(F^2)]$, $wR(F^2)$, S	0.046, 0.120, 1.01
no. of reflections, parameters, restraints	14307, 800, 0
H atom treatment	H atom parameters constrained
weighting scheme	$w = 1/[\sigma^2(F_0^2)+(0.0506P)^2+2.2167P]$ where $P = (F_0^2 + 2F_c^2)/3$
$\Delta\rangle_{max}$, $\Delta\rangle_{min}$ (e Å^{-3})	1.02, −0.41

One of the key requirements for the construction of such materials is a satisfactory separation of the molecules or chain polymers in solid to minimize the intermolecular interactions that preclude the manifestation of slow magnetic dynamics. There are two ways to eliminate these surplus contacts, namely, to use bulky capping[11g,15] and/or bridge ligand,[5,7h,q] or a voluminous counterion.[11g] The square planar complexes of Mn^{3+} with Schiff bases (SB), having significant easy axis anisotropy, are useful synthones in the synthesis of cyanide bridge alternate chains Fe^{III}−CN−Mn^{III}−NC− exhibiting SCM behavior.[14,15] Thus, any molecular wire based on the alternation of $[Fe(CN)_6]^{3-}$ and $[Mn(SB)]^+$ coordination units should be a SCM in the absence of interchain interactions. However, for the polymer complex $(Et_4N)_2[Mn(acacen)][Fe(CN)_6]$ (**1**) (Et_4N = tetraethylammonium, acacen = *N*,*N*′-ethylenebis(acetylacetonylideneaminato)),[16] relying on magnetic measurements data, the authors have concluded that **1** was a ferromagnet due to weak interchain ferromagnetic coupling. Motivated by this work, we decided to replace Et_4N^+ by a bulkier Ph_4P^+ cation to separate the chains better to unveil the SCM behavior in the $[Mn(acacen)Fe(CN)_6]^{2-}$ system. In this report we present the results of experimental and theoretical study of a new single chain magnet $(Ph_4P)_2[Mn(acacen)Fe(CN)_6](EtOH)_{0.5}$(*i*-PrOH) (**2**) and its congener $(Ph_4P)_2[Mn(acacen)Co(CN)_6](i\text{-PrOH})_{1.4}$ (**3**), and revision of the magnetic behavior of **1**, which appears not to be a ferromagnet as stated before.[16] Along with this, we discuss the origin of $[Fe(CN)_6]^{3-}$ anisotropy and its influence on the SCM parameters in **1** and **2**.

EXPERIMENTAL SECTION

Materials and General Procedures. All chemicals were of reagent grade and used as purchased. Schiff base, H_2acacen,[17] [Mn(acacen)Cl],[18a] and $[Et_4N]_2[Mn(acacen)][Fe(CN)_6]$[16] were prepared according to the literature procedures. Elemental analyses were performed by means of the Euro-Vector 3000 analyzer. IR spectra were recorded using Scimitar FTS 2000 spectrometer (KBr pellets) and Nicolet 300 FT-IR spectrometer in reflectance mode. Powder X-ray measurements were performed with Cu Kα radiation (λ = 1.5418 Å) with an Expert-Pro powder diffractometer. Magnetic measurements were performed using the QD MPMS 5XL magnetometer. The magnetic signal of the sample holder and the diamagnetic correction of the sample were taken into account. A check for small ferromagnetic impurities was performed at room temperature. The powder sample was restrained in cyanoacrylate glue for low temperature *ac* measurements. Magnetization measurements on single crystals were performed with a μ-SQUID array.[18b]

Synthesis. $(Et_4N)_2[Mn(acacen)][Fe(CN)_6]$ (1). **1** was synthesized as described earlier.[16] (Found: C, 54.35; H, 7.78; N, 18.70. $C_{34}H_{58}FeMnN_{10}O_2$ requires C, 54.47; H, 7.80; N, 18.68), $\nu_{(C=N-)}$ = 1601.6 cm^{-1}; ν_{CN} = 2124.5 cm^{-1} (KBr pellets).

$(Ph_4P)_2[Mn(acacen)][Fe(CN)_6]$ (2). A solution of $[Mn(acacen)(MeOH)_2]PF_6$ (0.2 mmol) in methanol (2 mL) was added to a solution of $(Ph_4P)_3[Fe(CN)_6]$ (236 mg) in ethanol (4 mL). Ph_4PPF_6, precipitated from reaction mixture, was filtered and discarded. The mother liquor was diluted with *i*-propanol (3 mL) and this solution was gently heated (without boiling) to evaporate the MeOH and EtOH. The brown block crystals were filtered, rinsed with a small amount of cold EtOH/*i*-PrOH (1/3) mixture and then with 2 portions of Et_2O, and air-dried. Yield: 216 mg (86%). (Found: C, 67.35; H 5.65; N, 9.01. $C_{70}H_{69}FeMnN_8O_{3.5}P_2$ requires C, 67.20; H, 5.56; N, 8.96), $\nu_{(C=N-)}$ = 1599.0, ν_{CN} = 2102.4 cm^{-1} (KBr pellets).

$(Ph_4P)_2[Mn(acacen)][Co(CN)_6]$ (3). A compound was synthesized by the same manner as **2** using $(Ph_4P)_3[Co(CN)_6]$ instead of $(Ph_4P)_3[Fe(CN)_6]$. Yield: 210 mg (84%) (Found: C, 67.40; H 5.60; N, 8.90. $C_{70.2}H_{66.4}CoMnN_8O_{3.4}P_2$ requires C, 67. 17; H, 5.56; N, 8.93%), $\nu_{(C=N-)}$ = 1598.7, ν_{CN} = 2113.4 cm^{-1}.

X-ray Crystallography. Crystallographic information for the structure of **2** are given in Table 1. The diffraction data were collected on a Bruker Apex DUO diffractometer with Mo Kα radiation (λ = 0.71073 Å) using φ and ω scans of narrow (0.5°) frames at 100 K. The

dx.doi.org/10.1021/ic501330j | Inorg. Chem. 2014, 53, 10291−10300

structure of **2** was solved by direct methods and refined by full-matrix least-squares method against $|F|^2$ in anisotropic approximation using SHELXTL programs set.[19] Absorption corrections were applied empirically using the SADABS program.[20] All non-hydrogen atoms were refined anisotropically.[21] Hydrogen atoms were refined in calculated positions using riding on pivot atom model. The hydrogen atom of the hydroxo group of the *i*-PrOH molecule was localized from the residual electron density map and refined with U_{iso} = 0.05; the *i*-propyl group is disordered over 2 close positions. The EtOH molecule occupies its position with 50% probability. Bond lengths and bond angles are summarized in Table S2 (see the Supporting Information). The hydrogen bonds were analyzed with TOPOS 4.0 program for crystal chemical analysis.[22]

Theoretical Calculations Details. Ligand-field (LF) calculations were performed in terms of a LF Hamiltonian for $[Fe^{III}(CN)_6]^{3-}$ complexes:

$$H = \sum_{i>j} \frac{e^2}{|r_i - r_j|} + \zeta_{Fe} \sum_i l_i s_i + V_{LF} + \mu_B(kL + 2S)\mathbf{H} \quad (1)$$

where the first term represents the Coulomb repulsion between the 3d electrons of Fe^{III} (*i* and *j* run over 3d electrons), the second term is the spin−orbit coupling (SOC) of Fe^{III}, V_{LF} is a ligand-field Hamiltonian, and the last term represents the Zeeman interaction with the external magnetic field **H**. In these calculations we use B = 720 and C = 3290 cm^{-1} Racah parameters for the Coulomb term, the SOC constant ζ_{Fe} = 345 cm^{-1}, and the k = 0.79 orbital reduction factor in the Zeeman term taken from literature.[23] The LF Hamiltonian V_{LF} is calculated in terms of the angular overlap model (AOM) with the AOM parameters e_σ = 9304 and e_π = −1779 cm^{-1} for the CN ligands obtained from ab initio calculations for $[Fe(CN)_6]^{3-}$;[23] the radial dependence of the AOM parameters is approximated by $e_{\sigma,\pi}(R) = e_{\sigma,\pi}(R_0)(R_0/R)^n$ with n = 3 and R_0 = 1.95 Å. Energy levels of the $3d^5$ LF states of $[Fe(CN)_6]^{3-}$ are obtained by a numerical diagonalization of the Hamiltonian (1) in the full set of $3d^5$ wave functions involving 252 $|LM_LSM_S\rangle$ microstates.

RESULTS AND DISCUSSION

Synthesis. Compound **1** was synthesized by exactly the same procedure as described in ref 16 and the data of IR, crystal cell, powder XRD (Figure S1−2, see the SI), CHN analysis confirmed that the sample was of good quality and corresponded well to the one reported[16] in 1996. A reaction of alcohol solutions of $[Mn(acacen)(CH_3OH)_2]PF_6$ and $(Ph_4P)_3[Fe(CN)_6]$ in ratio 1:1 gave a white precipitation of Ph_4PPF_6 that was removed by centrifugation. After dilution with *i*-propanol the reaction mixture was heated gently during 20 min to deliver the brown prismatic crystals of **2** suitable for single crystal X-ray diffraction. The diffractogram of the polycrystalline sample of **2** is in good agreement with the one calculated from the crystal structure (Figure S3, SI). Thermal analysis showed that complex **2** is stable up to ∼150 °C (Figure S4, SI). Compound **3** was synthesized similarly to **2**, using $(Ph_4P)_3[Co(CN)_6]$ instead of $(Ph_4P)_3[Fe(CN)_6]$. Complex **3** is isomorphic to **2** (see SI, Table S1, Figure S5).

Crystal Structure of 2. The X-ray structural study revealed that **2** is a 1D polymeric complex, containing one Mn ion in the general position and two symmetrically independent Fe ions in the inversion centers of the triclinic $P\bar{1}$ space group (Figure 1). For both nonequivalent Fe centers, the coordination environment of six CN-groups is an almost undistorted octahedron. All Fe−C bond distances vary within 0.015 Å and all bond angles NC−Fe−CN within 4° (Table 2). The coordination environment of the Mn ion is an elongated tetragonal bipyramid as a result of the Jahn−Teller distortion. The 2O and 2N donor atoms of the acacen ligand in the basal plane of the pyramid form shorter bonds of 1.89−1.97 Å, while two N atoms of

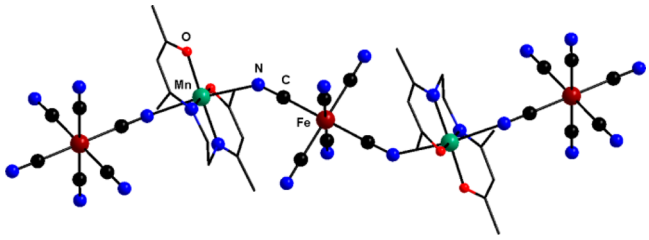

Figure 1. Fragment of a chain in **2**. Hydrogen atoms are omitted for clarity.

Table 2. Coordination Environment of Iron(III) and Manganese(III) Cations in 2[a,b]

bond	bond length, Å	bond angle	angle (deg)
Fe1—C1	1.951(3)	O11—Mn1—O21	91.13(7)
Fe1—C2	1.943 (2)	O11—Mn1—N21	175.45(8)
Fe1—C3	1.955(2)	O21—Mn1—N21	92.47(8)
		O11—Mn1—N11	92.03(8)
Fe2—C4	1.946(3)	O21—Mn1—N11	176.49(8)
Fe2—C5	1.947(3)	N21—Mn1—N11	84.45(8)
Fe2—C6	1.937(2)	O11—Mn1—N6	92.94(8)
		O21—Mn1—N6	93.38(7)
Mn1—N2	2.371(2)	N21—Mn1—N6	89.63(8)
Mn1—N6	2.298(2)	N11—Mn1—N6	84.92(8)
Mn1—O11	1.8925(17)	O11—Mn1—N2	93.07(7)
Mn1—O21	1.9053(17)	O21—Mn1—N2	92.58(7)
Mn1—N11	1.973(2)	N21—Mn1—N2	83.99(8)
Mn1—N21	1.970(2)	N11—Mn1—N2	88.79(8)
		N6—Mn1—N2	171.46(7)
bond angle	angle (deg)	bond angle	angle (deg)
C2—Fe1—C1^{i}	88.47(10)	C6—Fe2—C4	90.77(10)
C2—Fe1—C1	91.53(10)	C6—Fe2—C4^{ii}	89.23(10)
C2—Fe1—C3^{i}	91.69(9)	C6—Fe2—C5^{ii}	92.09(10)
C2—Fe1—C3	88.31(9)	C6^{ii}—Fe2—C5^{ii}	87.91(10)
C1—Fe1—C3	89.23(10)	C4—Fe2—C5^{ii}	90.11(12)
C1—Fe1—C3^{i}	90.76(10)	C4—Fe2—C5	89.89(11)

[a]The numbering scheme (see Figure S6, SI). [b]Symmetry codes corresponding to inversion centers (i) $-x+1, -y+1, -z+1$, and (ii) $-x+2, -y+2, -z+2$.

trans-disposed CN ligands form much longer (2.29−2.37 Å) Mn−N_{CN} bonds and $_{NC}$N−Mn−N_{CN} angle of 171.5° (Table 2). Apical sites of the Mn ion in the $[Mn(acacen)]^+$ are occupied by CN groups in trans positions of the $[Fe(CN)_6]^{3-}$ octahedra, forming a repeating unit of a chain. The Mn−N−C bond angles are much lower than 180° and equal to 142.8° and 148.6°, being typical of the cyanide bridged Mn^{III}−Fe complexes[11a,24,25] that results in a zigzag chain motif.

In **2**, the chains run along the {111} crystallographic direction (Figure S7a, SI) and are separated by bulky Ph_4P^+ cations and *i*-PrOH and EtOH solvent molecules. This leads to the shortest interchain distance d between Mn centers of 11.38 Å compared with shorter 10.41 and 10.08 Å in **1** and in neutral $[Mn(5TMAMsalen)Fe(CN)_6]\cdot 4H_2O$ (**4**),[15] respectively. Similarly to **1** and **4**, in a crystal of **2**, the parallel zigzag chains form hexagonal rod packing[26] (Figure S7b, SI).

The geometry of the zigzag chain skeleton in **1**, **2** and **4** built up by lineal NC−Fe−CN and essentially linear N−Mn-(acacen)−N units differ in ∠C−N−Mn angles at every nitrogen atom of the CN group. It is essential to note that the Jahn−Teller axes of the [Mn(SB)] units are codirectional

dx.doi.org/10.1021/ic501330j | Inorg. Chem. 2014, 53, 10291−10300

with the chain. Among the three compounds, **2** has the most bent chain skeleton (Figure S7c, SI).

In **2**, each Fe center carries four terminal CN-groups able to form a hydrogen bond; two of these four cyanide ligands are sterically hindered by Ph_4P^+ cations and do not participate in hydrogen bonding (HB). In contrast to **1**, which is solvent-free, the other two CN-groups form the RO−H···N≡C bonds alternatively with solvated RO−H, R = *i*-Pr or Et (Figure S8, Table S3, SI). The *i*-PrOH molecule participates in the long O···N hydrogen bond of 3.041(6) Å and separates Ph_4P^+ moieties in the *b* direction (Figure S8). A shorter hydrogen bond of O···N 2.866(3) Å is formed by the ethanol molecule, which is disordered so that it belongs alternatively to one of the two neighboring chains along the axis *a*. The oxygen atoms of the acacen ligand do not participate in HB. Therefore, there is no HB network involving nearest chains. The closest interchain contact in **2** is found between the nitrogen atom (N5) of the cyano group and the carbon atom (C21) of the acacen ligand with the approximate distance 6.71 Å.

Magnetic Studies of 2. Along with the experimental data for **2** presented in this section, the corresponding results for **1** are also shown in the figures. However, the description and analyses for **1** are given in the next section for clarity, and to emphasize the original results.

The magnetic susceptibility is shown in Figure 2 as the χT product. At 300 K, χT = 3.43 cm^3K/mol, which corresponds

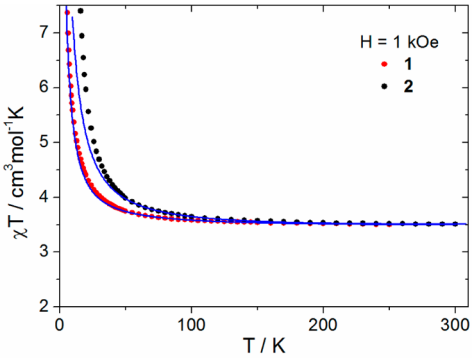

Figure 2. Magnetic susceptibility of **1** (red) and **2** (black). Lines were fitted according to the Seiden's model.

well to the Curie constant of 3.38 cm^3K/mol expected for two noninteracting spins: Fe^{III}, described by S_{Fe} = 1/2, g_{Fe} = 2, and Mn^{III} with S_{Mn} = 2, g_{Mn} = 2. As the temperature decreases, χT rises gradually, without a minimum, testifying the dominance of ferromagnetic interactions between the Fe and Mn centers. The model of an alternating chain composed of Heisenberg spins 1/2 and 2 and defined by the Hamiltonian $\hat{H} = -2J\sum_i(S^i_{Mn} + S^{i+1}_{Mn})\cdot S^i_{Fe}$, was used to estimate the coupling constant *J*. A solution of this Hamiltonian, in the approximation that spins *S* are treated classically, was obtained by Seiden as an analytical formula for susceptibility.[27] For **2**, a single *J* value was assumed, identical for all Fe−Mn pairs, and g_{Fe} = 2 was fixed. Using the data in the range of 50−300 K, g_{Mn} = 1.98(1) and J/k_B = +6.7(2) K was obtained for **2**. The data points below 50 K deviate from the calculated curve. An attempt to improve the model in the mean field approximation by introducing an additional coupling parameter responsible for interchain interaction failed because it led to an unacceptably high zJ' value of the same order as *J*.

Below 10 K the susceptibility χ rises much quicker, and below 5 K it saturates when measured at 1 kOe, and depends on the applied field (Figure S9, SI). Thus, low-field measurements were used to analyze the low temperature susceptibility. The anisotropy of Mn^{III} spins, originating from zero-field splitting, makes the Seiden's approximation no longer valid for **2** at low temperatures. Anisotropic 1D magnetic systems have a gap in the spin excitation energy spectrum, which leads to the susceptibility dependence[7]

$$\chi T = C_{eff}\exp(\Delta_\xi / T)$$

In this equation C_{eff} is an effective Curie constant, which in our case takes into account the averaging of anisotropic magnetic susceptibility in the powder sample as well. Δ_ξ denotes the energy of the domain wall, which is the lowest excitation of the ground state in the chain of correlated spins. To estimate Δ_ξ, the susceptibility data were plotted as $\ln(\chi T)$ vs T^{-1} (Figure 3).

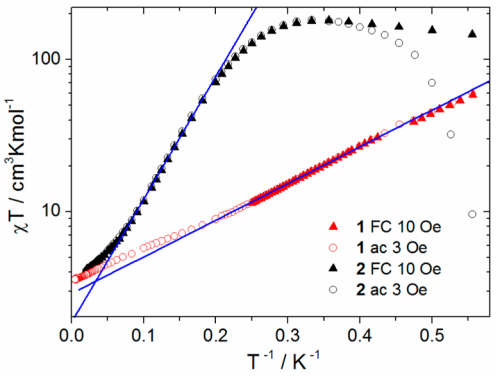

Figure 3. Magnetic susceptibility of **1** (red) and **2** (black), dc and ac, measured at low field. Straight lines were fitted (see text).

The points denoting the ac susceptibility were measured at H_{ac} = 3 Oe, 0.1 Hz, H_{dc} = 0, and points denoting the field cooled dc susceptibility were measured at H_{dc} = 10 Oe overlap above 3 K. The linear part of the ac susceptibility in the region from 5 to 10 K was used to obtain Δ_ξ/k_B = 18.5(2) K and C_{eff} = 1.89 cm^3K/mol.

For experimentally studied SCMs below a certain temperature the $\chi T(1/T)$ dependence deviates from the exponential divergence and saturates, even for a low applied field, due to the finite chain length caused by crystal defects.[7] This happens when the growing correlation length exceeds the average chain length *n*. For **2** it is visible below 3 K, where $(\chi T)_{max}$ = 180 cm^3K/mol. The average chain length estimation using the relation $(\chi T)_{max} = nC_{eff}$, gave $n \geq 95$ Fe−Mn units. However, such an estimation of *n* should be treated with care, because two other effects can also decrease the measured susceptibility in this temperature range: (a) possible antiferromagnetic interchain interaction and (b) demagnetization leading to a decrease of the measured χ. For this reason the estimation given above is a lower limit of *n*.

Below 3 K the *ac* susceptibility (Figure 3) deviates from the field-cooling *dc* susceptibility indicating slow magnetization relaxation. In Figure 4, the temperature dependence of the ac susceptibility measured at zero dc field for different ac field frequencies is presented. The imaginary part of the *ac* susceptibility $\chi''(T)$ has a maximum below 4 K. Its exact position, shifting with the change of the *ac* drive field frequency υ, retains the shape that is usual for a temperature induced

dx.doi.org/10.1021/ic501330j | Inorg. Chem. 2014, 53, 10291−10300

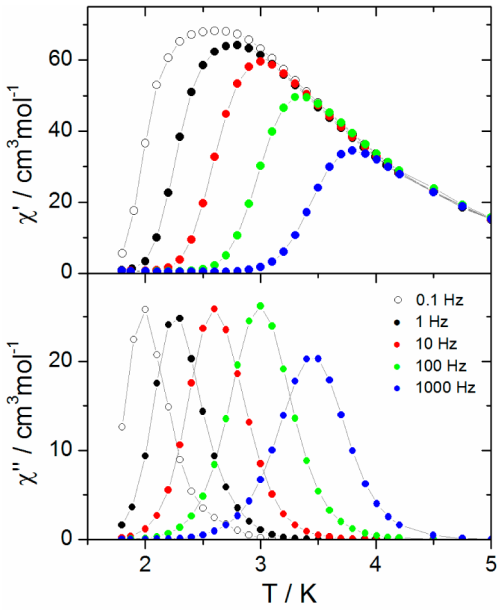

Figure 4. Real and imaginary part of ac susceptibility of **2** measured at different ac frequencies using H_{ac} = 3 Oe in zero dc field. Solid lines are to guide the eye.

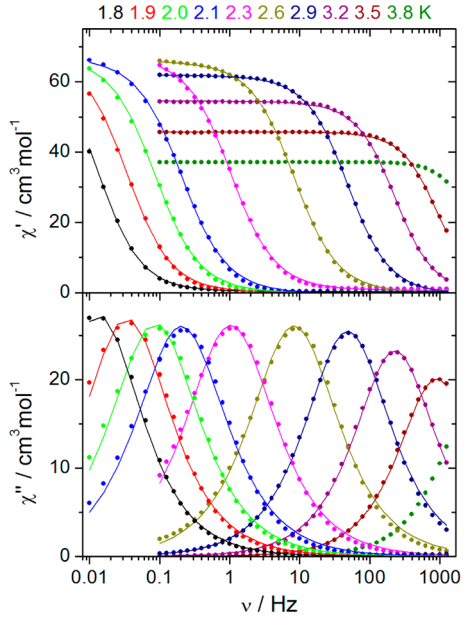

Figure 5. ac susceptibility measured for **2** at selected temperatures versus ac frequency ν. Solid lines were fitted using a generalized Debye relaxation model, simultaneously to $\chi'(\nu)$ and $\chi''(\nu)$ curves.

relaxation process. The Mydosh parameter, defined as the temperature shift of $\chi'(T)$ peak position on a decade of frequency $\Delta T_m/[T_m \Delta \log(\upsilon)]$, is equal to 0.10. Such a value is above the range typical for spin-glasses and closer to the values for superparamagnets.[28]

To obtain a better insight into the magnetic relaxation processes the *ac* susceptibility was studied over the frequency range 0.01−1500 Hz and down to 1.8 K; the data are presented in Figure 4. The frequency dependent susceptibility measured at constant temperatures was used to determine the relaxation time at each temperature. The generalized Debye relaxation model[29]

$$\chi = \chi' - i\chi'' = \chi_\infty + \frac{\chi_0 - \chi_\infty}{1 + (i2\pi\nu\tau)^{1-\alpha}}$$

was used to fit $\chi'(\upsilon)$ and $\chi''(\upsilon)$ simultaneously (Figures 5 and S10). At each temperature the fitted parameters were: χ_0 and χ_∞, the relaxation time τ and the parameter α, describing the distribution of relaxation times. Small α values in the range 0.07−0.16 were obtained (Table S4, SI), confirming the good quality of the sample and indicating the SCM nature of **2**.

The relaxation times in the temperature range from 1.8 to 3.8 K, obtained from the ac susceptibility analysis, are presented in Figure 6. The dependence ln $\tau(1/T)$ deviates from the straight line of the Arrhenius law. This is a feature of experimentally studied SCMs with finite chains, for which, below the crossover temperature T^*, the probability of relaxation arising from the ends of chains becomes important, changing the relaxation barrier.[7] Above T^*, where the correlation length ξ is lower than the average chain length $L = na$, the relaxation barrier is equal to $\Delta_{\tau 1} = \Delta_A + 2\Delta_\xi$, where Δ_A is the anisotropy energy of a single spin unit. Below T^*, the relaxation barrier is reduced and equal $\Delta_{\tau 2} = \Delta_{\tau 1} - \Delta_\xi$ in the low temperature limit. The values of $\Delta_{\tau 1}$ and $\Delta_{\tau 2}$ are usually obtained from two linear regions of the ln$\tau(1/T)$ dependence much above, and much below T^*, respectively. In the case of **2**, the limited range of relaxation times available from the ac experiment makes such determination more difficult. To obtain both relaxation barriers using all data points, also close to T^*, we used the relation derived by Luscombe et al. for the finite Ising chain.[30] The finite length L of the chain shortens the relaxation time by the factor $f(L/\xi)$:

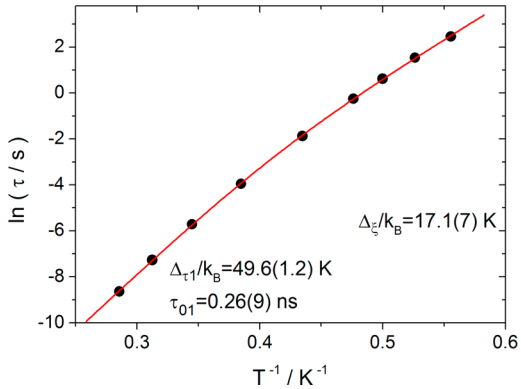

Figure 6. Relaxation time of ac susceptibility for **2**, the curve was fitted (see text).

$$\tau = \tau_{01} \exp\left(\frac{\Delta_{\tau 1}}{k_B T}\right) f(L/\xi) \quad (2)$$

where $f(x) = (1 + w^2/x^2)^{-1}$, and w is the solution of the equation

$$w \tan(w/2) = x \quad (3)$$

in the $[0,\pi)$ range. Together with temperature dependence of the correlation length

$$\xi = \frac{a}{2} \exp\left(\frac{\Delta_\xi}{k_B T}\right)$$

Equation 2 allows us to calculate $\tau(T)$ as the function of parameters Δ_ξ, $\Delta_{\tau 1}$, τ_{01}, and L/a. eq 3 was solved numerically using the bisection method for $x > 10^{-3}$, while the

dx.doi.org/10.1021/ic501330j | Inorg. Chem. 2014, 53, 10291−10300

approximation $w = (2x)^{1/2}$ was used for small values of $x < 10^{-3}$. The parameters $\tau_{01} = 0.26(9)$ ns, $\Delta_{\tau 1}/k_B = 49.6(1.2)$ K, $\Delta_\xi/k_B = 17.1(7)$ K and $L/a = 1500(500)$ were found fitting to experimental data points (see Figure 6). This Δ_ξ is very close to the domain wall energy in the chain $\Delta_\xi/k_B = 18.5$ K, determined earlier from $\ln(\chi T)(1/T)$. The obtained values let us to estimate the anisotropy barrier $\Delta_A/k_B = (\Delta_{\tau 1} - 2\Delta_\xi)/k_B = 15$ K.

The average chain length of 1500 Fe−Mn units determined here is over 10 times higher than the same chain length determined from static magnetic measurements. Similar observation is made in other SCMs, e.g. Mn^{III}-M^{III} chains.[15] Such a disagreement may be related to weak antiferromagnetic interaction between chains, which reduces the susceptibility at low temperatures and falsifies the chain length determination from static measurements. In Mn−Fe chains the anisotropy easy axis of Mn is along chains, therefore the dipolar interaction between chains should be antiferromagnetic.

The field dependence of magnetization measured at 1.8 K for **2** increases rapidly to 2.8 μ_B/(FeMn-unit) at 1 kOe (Figure S11, SI). For a set of Ising spins arranged along their easy axes in randomly oriented crystallites the saturation magnetization value is smaller by a factor 0.5 compared with the saturation magnetization along the easy axis for all spins. Therefore, starting from the maximal magnetization 5 μ_B of a single Mn−Fe unit, only 2.5 μ_B can be expected for a powder sample in the field small enough to retain the Ising easy axis, and high enough to overcome the demagnetization and possible interchain interactions. This explains the measured 2.8 μ_B value. The slow increase of $M(H)$ for **2** at higher fields allows a rough estimation of the anisotropy field $H_A \approx 120$ kOe, obtained by an extrapolation of the measured data up to 5 μ_B. Assuming that the Mn^{III} zero field splitting is the only source of the magnetic anisotropy, the anisotropy parameter $D_{Mn}/k_B = -5.0$ K based on $2|D_{Mn}|S_{Mn}^2 = g\mu_B H_A(S_{Mn} + S_{Fe})$.

An independent measurement of D_{Mn} was performed from the magnetic study of complex **3**, in which Co^{III} takes the place of Fe^{III}. The $3d^6$ configuration of Co in the octahedral crystal field ensures the diamagnetic ground state with a completely occupied t_{2g} level. In this case, the magnetic moment of **3** derives only from the $[Mn^{III}(acacen)]^+$ cations. Their effective separation by nonmagnetic $[Co(CN)_6]^{3-}$ anions allows the determination of the Mn^{III} single ion magnetic properties. The analysis of the magnetic data (Figure S13, SI) leads to $D_{Mn}/k_B = -4.78(4)$ K. This value is expected to be similar to the one for **2** because both compounds are isostructural.

The comparison of Δ_ξ and Δ_A shows that **2** seems to be just beyond the Ising limit of single chain magnets, because $\Delta_\xi > \Delta_A$. An estimation in the Ising model of an alternating chain delivers $\Delta_\xi^{Ising}/k_B = 4JS_{Mn}S_{Fe} = 26$ K. For the Heisenberg model in the continuum-limit approximation $\Delta_\xi^{Heis}k_B = 2(2D_{Mn}JS_{Mn}^3S_{Fe})^{1/2} = 29$ K. Both values are larger than $\Delta_\xi/k_B = 18.5$ K measured for **2**.

Magnetic Properties of 1. For a sample of **1**, we have repeated the magnetic measurements of Re et al. resulting in almost identical $\chi T(T)$ and $M(H)$ curves as reported[16] (Figures 2 and S11). No magnetic ordering was observed above 1.8 K, contrary to the published results.[16] As the first magnetic study of **1** was performed before the discovery of SCMs, the data for **1** were analyzed using the same approach as for **2**. The Seiden's model fit for **1** over the temperature range 50−250 K delivers $J/k_B = 3.48(7)$ K and $g = 2.01(2)$. The curve calculated using these parameters reproduces χT well down to ∼5 K (Figure 2). Additionally, low field measurements were performed. At low temperatures the susceptibility of **1** is significantly smaller than the susceptibility of **2**, e.g. by is a factor above 10 at 4 K. The linear fit to the $\ln(\chi T)$ vs T^{-1} in the range 2.5−5 K provides the estimation of $\Delta_\xi/k_B = 5.55(2)$ K (Figure 3). The study of ac susceptibility for **1** (Figure 7) shows a tiny nonzero frequency dependent out-of-phase signal below 2.1 K, affirming that SCM behavior might also be observed for **1** below 1.8 K.

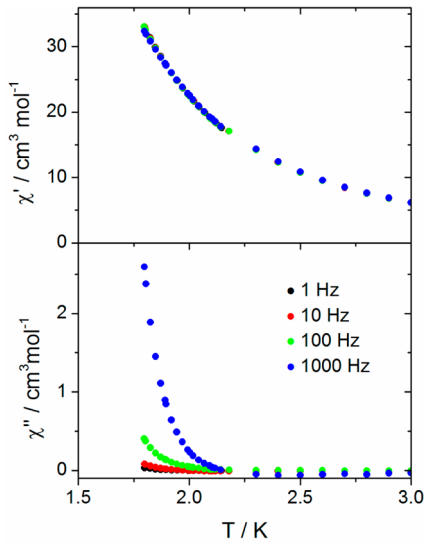

Figure 7. Magnetic ac susceptibility of **1**, measured at zero dc field, and $H_{ac} = 3$ Oe.

The appearance of slow relaxations in **1** was confirmed using microSQUID setup[31] and measuring the magnetization of a single crystal down to 0.4 K. The hysteresis loop opens below 1.0 K and its coercive field grows with decreasing temperature (Figure 8, top) and with increasing sweep rate (not shown). There are no additional steps on $M(H)$ curve. Such a behavior is expected for SCMs, contrary to SMMs, where the quantum tunneling leads to a quicker relaxation at the specific fields. For comparison similar measurements were performed for a single crystal of **2**, which is also shown in Figure 8. In this case the hysteresis loop opens already at 2.4 K, when the field sweep rate is 0.14 T/s. Below 0.7 K the coercive field no longer grows and remains constant down to 0.03 K. Again, this effect is typically observed for SCMs.[15]

Comparison of SCM Parameters of 1, 2, and 4. The parameters related to SCM behavior of **1** and **2** are summarized in Table 3 and compared with those of **4**.[15] A study of **1** below 2 K is needed to determine all magnetic parameters for this compound. Why does **2** display SCM behavior at a higher temperature compared to **1** if both compounds are related polymers, having similar intrachain bond lengths? The differences in interchain coupling can be neglected because d, the distance between the Mn ions in adjacent chains, is larger than 10 Å in all three Mn^{III}−NC−Fe^{III}−CN− polymers (Table 3), the shortest d occurring in the neutral chain **4**, which is also a SCM above 2 K (see above). The stronger exchange interaction could be one of the reasons for higher blocking temperatures of **2**. For **2** and **4**, Δ_ξ values found using J and D in Ising or Heisenberg limits overestimates the measured values of Δ_ξ. Similarly, for **1** Δ_ξ can be compared with the value estimated from the J value of the Seiden model. In this case the Ising limit seems to be appropriate, since the anisotropy is

dx.doi.org/10.1021/ic501330j | Inorg. Chem. 2014, 53, 10291−10300

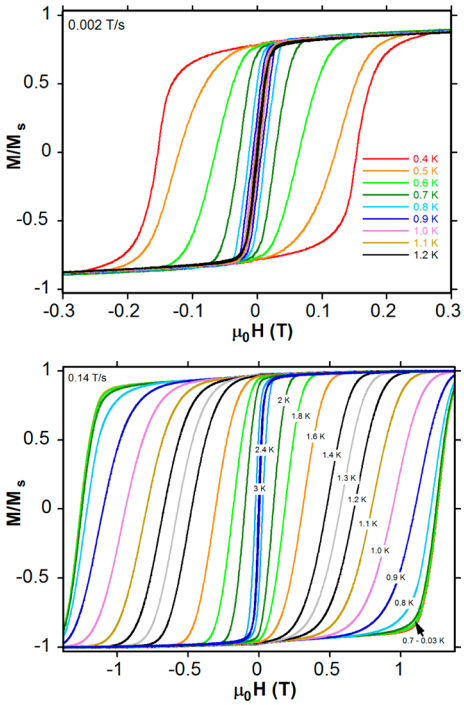

Figure 8. Normalized magnetization of a single crystal of **1** (top) and a single crystal of **2** (bottom) measured at different temperature. Note the different field sweep rates and different horizontal scales.

similar as in **2**, but the exchange constant is smaller. However, the calculated value Δ_ξ^{Ising}/k_B = 14 K in this case, which is almost three times bigger than Δ_ξ obtained from the low temperature susceptibility. The most probably the Seiden expression does not describe well this compound, as it also does not model correctly the chain **2** and the obtained value of J is biased. Finally, in **2**, a lower value of D_{Mn} is anyway compensated resulting in a higher H_A. This is due to a larger contribution of $[Fe(CN)_6]^{3-}$ anisotropy displaying also at high temperatures (see below) which is a possible explanation. To check for this we performed the calculations of the electron structure of the Fe ion in these compounds.

Comparative Ligand-Field Calculations for $[Fe^{III}(CN)_6]^{3-}$ Complexes in 1, 2, and 4. The real situation with magnetic exchange interactions in alternating cyano-bridged Fe–Mn chains complexes seems to be much more complicated, since the octahedral $[Fe(CN)_6]^{3-}$ complex is an orbitally degenerate unit with unquenched orbital momentum L in the $^2T_{2g}$ ground state. In this case, both the g_{Fe} tensor and the spin coupling in the Fe^{III}–CN-Mn^{III} pairs may be essentially anisotropic. Magnetic anisotropy of $[Fe(CN)_6]^{3-}$ based compounds may be sensitive even to tiny coordination octahedron distortions, which split the $^2T_{2g}$ triplet into individual orbital components (Figure 9) and thus tend to reduce L. It should be noted that L is unquenched when the energy gap between the lowest and the next orbital components

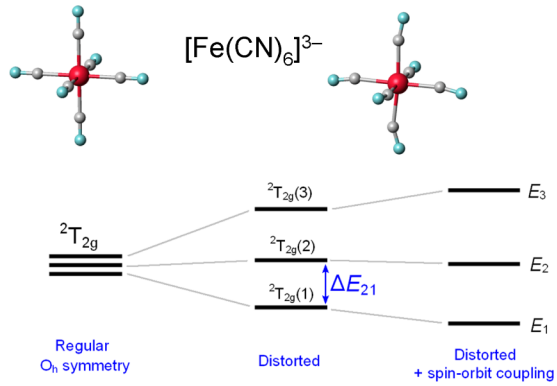

Figure 9. Splitting of the ground orbital triplet $^2T_{2g}$ in distorted $[Fe(CN)_6]^{3-}$ complex.

(ΔE_{21}) is lower than or comparable with the spin–orbit coupling energy, ζ_{Fe}. To examine this point in more detail, ligand-field calculations for local ferricyanide anions in **1**, **2**, and **4** were performed. The calculated energies of the individual orbital components $^2T_{2g}(1)$, $^2T_{2g}(2)$, $^2T_{2g}(3)$, the energies of three lowest Kramers doublets (Figure 9) and the ground state g tensor components are presented in Table 4. The presented

Table 4. Calculated Orbital Splitting Pattern of the Ground Orbital Triplet $^2T_{2g}(3d^5)$, Energies of the Ground and Two First Excited Kramers Doublets, and Ground-State g-Tensor Components of $[Fe(CN)_6]^{3-}$ in 1, 2, and 4

	1	2		4
		Fe1	Fe2	
Energy (cm^{-1}) of the Orbital Components of the Ground Orbital Triplet $^2T_{2g}$				
$E(^2T_{2g}(1))$	0	0	0	0
$E(^2T_{2g}(2))$	363	506	312	561
$E(^2T_{2g}(3))$	888	638	600	998
Energy (cm^{-1}) of the Ground and Two First Excited Kramers Doublets				
E_1	0	0	0	0
E_2	598	671	579	721
E_3	1126	933	899	1206
g-Tensor Components of the Ground Kramers Doublet				
g_1	0.623	0.680	0.198	1.080
g_2	2.033	2.450	2.151	2.296
g_3	3.205	2.812	3.026	2.976

results indicate that in **2** the $^2T_{2g}$ term splitting energy is slightly smaller than in **1** and **4**. It is especially visible in the case of the Fe2 center, in which the energy gap ΔE_{21} = 312 cm^{-1} is lower than the ζ_{Fe} = 345 cm^{-1} for $[Fe(CN)_6]^{3-}$. This means that L remains mainly unquenched in **2**. As a result, the Fe^{III}–CN-Mn^{III} spin coupling in **2** should have a pronounced anisotropy, which favors the enhanced SCM parameters of **2**. It should be noted that the current calculations were performed using the geometrical parameters taken from single crystal X-ray diffraction data collected at different temperatures (Table 5)

Table 3. Single Chain Magnet Related Parameters for 1, 2, and 4

	d^a (Å)	J/k_B (K)	Δ_ξ/k_B (K)	H_A (kOe)	Δ_ξ^{Ising}/k_B (K)	Δ_ξ^{Heis}/k_B (K)	Δ_{r1}/k_B (K)	Δ_{r2}/k_B (K)	Δ_A/k_B (K)	D_{Mn}/k_B (K)
1	10.41	3.48	5.55		14					
2	11.38	6.5	18.5	120	26	29	50	32.5	15	−4.78
4[15]	10.08	4.5	14.1	108	18	28	32	16	≈0	−5.3

[a]The shortest distance between Mn ions of adjacent chains.

dx.doi.org/10.1021/ic501330j | Inorg. Chem. 2014, 53, 10291–10300

Table 5. Selected Bond Length and Angles for −NC−Fe−CN−Mn−NC−Fe− Fragment in 1, 2, and 4

	T^a (K)	∠C−N−Mn (deg)	∠CN−Mn−NC (deg)	Fe−CN (Å)	Mn−NC (Å)
1[16]	294	152.6	172.0	1.958	2.316(4)
2	100	142.8[b]	171.41	1.944[b]	2.371(2)[b]
		148.7[c]		1.938[c]	2.298(2)[c]
4[15]	150	144.4	170.80	1.944	2.307(3)

[a]The temperature of SC-XRD study. [b]For Fe1. [c]For Fe2.

and aim only to illustrate the extreme sensitivity of orbital splitting energies to slight distortions of ferricyanide octahedron. Indeed, it would be more correct to use the atomic coordinates obtained at liquid helium temperatures.

Magneto-Structural Correlations. It is important to note that the correlations discussed below should be treated with caution because the structural parameters are very sensitive to temperatures at which they were determined.

The structural characteristics of the local environment in the −NC−Fe−CN−Mn−NC−Fe− fragment of chemically related complexes **1**, **2**, and **4** are presented in Table 5 and illustrated in Figure S7c. It should be underlined that both **1** and **2** are composed of polyanionic chains and cations, while **4** represents a neutral 1D coordination polymer with solvated water molecules. In solid state the paramagnetic chain skeletons are effectively separated from each other due to the organic cations in **1**, **2**, and bulky trimethylammonium groups of SB ligands in **4**. The bond lengths and CN−Mn−NC angle values within the chain skeleton are close for **1**, **2**, and **4**. As shown above, the main distinctive feature of **2** is the presence of two independent $[Fe(CN)_6]^{3-}$ complexes in the crystal asymmetric unit, while in **1** and **4** all $[Fe(CN)_6]^{3-}$ anions are equivalent. The presence of the voluminous Ph_4P^+ cations in **2** might be the reason for the lowering of the crystallographic symmetry from *Pnma* (in **1**) and *C*2/*c* (in **4**) to $P\bar{1}$. This causes some distortions of the chain skeleton of **2**, resulting in two crystallographically nonequivalent Fe centers with differently distorted environment and linked by the $[Mn^{III}(acacen)]^+$ complex with unequal apical Mn−N(C) distances (Table 2) in contrast with **1**[16] and **4**.[15]

The analysis of intrachain geometry together with the results of the ligand-field calculations allow us to summarize that the presence of two differently distorted $[Fe(CN)_6]^{3-}$ complexes could cause the additional anisotropy in **2** compared to **1** and **4**. In addition, the presence of two nonequivalent iron centers complicates the situation with the exchange interactions in **2** considerably, making the model using only one coupling constant J_{MnFe} non valid.

The exchange interaction was found to be ferromagnetic in all the three complexes. Ferromagnetic coupling occurs as a result of the rigorous orthogonality of the t_{2g} orbitals of iron(III) (d_{xz}, d_{yz}, d_{xy}) with the *eg* orbital (d_{z^2}) in manganese(III),[32] while the overlap between the t_{2g} orbitals of the two centers leads to antiferromagnetic interaction.[33] The total magnetic behavior of the Fe^{III}−Mn^{III} unit depends on which contribution is predominant. It is important that the ground level $^2T_{2g}$ (**1**) of $[Fe(CN)_6]^{3-}$ is a mixture of the three orbital components $^2T_{2g(xy)}$, $^2T_{2g(xz)}$, and $^2T_{2g(yz)}$ of the $^2T_{2g}$ orbital triplet; the mixture coefficients and the resulting exchange parameters may be very sensitive to the local distortions of the $[Fe(CN)_6]^{3-}$ complex (see Figure 9).

An exhaustive analysis of the $[Mn^{III}(SB)]_n[Fe^{III}(CN)_6]$ complexes known to date and the results of the DFT calculations performed by Kara et al.[13d] show that two factors are crucial, namely, the bending angle in the C−N−Mn group and the relative rotation of the local *x* and *y* axes on the Fe and Mn centers. The latter significantly reduces the overlap between the d_{xz}(Mn) and d_{xz}(Fe) orbitals, as well as between the d_{yz}(Mn) and d_{yz}(Fe) ones, favoring the ferromagnetic contribution. On the other hand, the bending angle removes the strict orthogonality of the t_{2g} and e_g orbitals on the metal atoms, thus introducing new antiferromagnetic pathways. However, it has been suggested that the increase of bending should reduce the overlap between the magnetic orbitals, finally leading to a decrease of the antiferromagnetic contribution.[13b,34] The C−N−Mn bond angles lower than ∼160° result in ferromagnetic coupling for this type of systems, while more obtuse angles may result in antiferromagnetic coupling. These conclusions are also supported by our results. The coupling constants, estimated by fitting of the experimental data, are 3.48, 4.5,[15] and 6.5 K for **1**, **4**, and **2** respectively. Despite these values being sufficiently close, they grow with the decrease of the C−N−Mn angle. This is especially visible for the Fe2 center in **2** having the least angle of 142.81° compared to 152.6 and 144.4° for **1** and **4** respectively (Table 5). On the other hand, the real situation with the sign and magnitude of exchange parameters in **1**, **2**, and **4** may be more complicated due to the presence of unquenched orbital momentum and first-order spin−orbit coupling on the $[Fe(CN)_6]^{3-}$ complexes. These features should result in anisotropic Fe^{III}−Mn^{III} spin coupling and some spin canting; their manifestation in the overall magnetic behavior can be very similar to conventional isotropic ferromagnetic spin coupling. However, detailed analysis of these anisotropic magnetic effects is out of scope of this work.

CONCLUSIONS

It can be stated that the cation plays some templating role in the SCM properties tuning of Mn−Fe chains **1** and **2**, since for the closest packing formation the chain polyanions have to be arranged around their counterparts. A replacement of the cation leaves the intrachain bond lengths mostly undisturbed, but modifies the distortion of the coordination polyhedron of the iron ion that affects the orbital splitting energy of the ferricyanide ground triplet $^2T_{2g}$, either quenching the orbital momentum or not. Hence, the extent of the L_{Fe} quenching determines, together with ZFS parameter D_{Mn}, the magnetic anisotropy in alternating Mn^{III}−Fe^{III} chains. The more pronounced contribution of hexametallate orbital momentum in the magnetic anisotropy was demonstrated recently in the case of the related Mn^{III}−Os^{III} SCM, $(Ph_4P)_2[Mn(acacen)Os(CN)_6](H_2O)_{1.5}(C_3H_7O)_{0.7}$.[35] The deviation of $\chi T(T)$ for **2** from its fit below 50 K clearly shows that the data cannot be modeled using the Seiden's approximation. Moreover, the measured value of Δ_ξ is fairly lower than those estimated assuming only the Mn^{III} anisotropy and determined exchange constant. In addition, there is no appropriate theoretical model for such a complicated chain system.

ASSOCIATED CONTENT

Supporting Information

Crystallographic details (CIF), supplementary tables, and figures for additional structural and magnetic data. This

material is available free of charge via the Internet at http://pubs.acs.org.

AUTHOR INFORMATION

Corresponding Authors

*E-mail: vosk@niic.nsc.ru.

*E-mail: m.rams@uj.edu.pl.

Notes

The authors declare no competing financial interests.

ACKNOWLEDGMENTS

This work was supported in part by RFBR (Grant 08-03-00459-a) and REA (FP7-PEOPLE-2011-IIF Proposal 301689). Magnetic measurements were carried out with the equipment purchased with support of the European Regional Development Fund in the framework of the Polish Innovation Economy Operational Program (POIG.02.01.00-12-023/08).

REFERENCES

(1) (a) Kahn, O. *Molecular Magnetism*; VCH: New York, 1993. (b) *Molecular Magnetism: From Molecular Assemblies to the Device*; Coronado, E., Delhaes, P., Gatteschi, D., Miller, J. S., Eds.; NATO ASI Series: Washington, DC, 1995. (N) *Magnetism: Molecules to Materials (I–V)*; Miller, J. S., Drillon, M., Eds.; Wiley-VCH: Weinheim, Germany, 2002–2005. (c) Thompson, L. K. *Coord. Chem. Rev.* **2005**, *249*, 2549. (d) Coronado, E.; Dunbar, K. R. *Inorg. Chem.* **2009**, *48*, 3293. (e) Brechin, E. K., Ed.; Themed issue on Molecular Magnetism, *Dalton Trans.* **2010**, *39*, 4671.

(2) (a) Coronado, E.; Day, P. *Chem. Rev.* **2004**, *104*, 5419. (b) Ehrenstein, W.; Mathur, N. D.; Scott, J. F. *Nature* **2006**, *442*, 759. (c) Sato, O.; Tao, J.; Zhang, Y. Z. *Angew. Chem., Int. Ed.* **2007**, *46*, 2152. (d) Bogani, L.; Wernsdorfer, W. *Nat. Mater.* **2008**, *7*, 179. (e) Coronado, E.; Martí-Gastaldo, C.; Navarro-Moratalla, E.; Ribera, A.; Blundell, S. J.; Baker, P. J. *Nat. Chem.* **2011**, *2*, 1031.

(3) Dunbar, K. R. *Inorg. Chem.* **2012**, *51*, 12055.

(4) (a) Gatteschi, D.; Sessoli, R.; Villain, J. *Molecular Nanomagnets*; Oxford University Press: New York, 2006. (b) Molecular Magnets: Physics and Applications. In *Struct. Bonding (Berlin)*; Juan, B., Fernando, L., Fernández, J. F., Ed.; Springer: New York, 2014, and references therein.

(5) Caneschi, A.; Gatteschi, D.; Lalioti, N.; Sangregorio, C.; Sessoli, R.; Venturi, G.; Vindigni, A.; Rettori, A.; Pini, M. G.; Novak, M. A. *Angew. Chem., Int. Ed.* **2001**, *40*, 1760–1763.

(6) For the reviews see: (a) Lescouëzec, R.; Toma, L. M.; Vaissermann, J.; Verdaguer, M.; Delgado, F. S.; Ruiz-Pérez, C.; Lloret, F.; Julve, M. *Coord. Chem. Rev.* **2005**, *249*, 2691–2729. (b) Miyasaka, H.; Clerac, R. *Bull. Chem. Soc. Jpn.* **2005**, *78*, 1725–1748. (c) Miyasaka, H.; Julve, M.; Yamashita, M.; Clérac, R. *Inorg. Chem.* **2009**, *48*, 3420–3437. (d) Sun, H.-L.; Wang, Z.-M.; Gao, S. *Coord. Chem. Rev.* **2010**, *254*, 1081–1100. (e) Wang, S.; Ding, X.-H.; Li, Y.-H.; Huang, W. *Coord. Chem. Rev.* **2012**, *256*, 439–464. (f) Kang, L.-C.; Zuo, J.-L. *Multifunctional Molecular Materials*; Ouahab, L., Ed.; Pan Stanford Publishing: Singapore, 2013; pp 105–131. (g) Zhang, W.-X.; Breedlove, B.; Ishikawa, R.; Yamashita, M. *RSC Adv.* **2013**, *3*, 3772–98. (h) Gatteschi, D.; Vindigni, A. Single-Chain Magnets. In *Struct. Bond.*; Juan, B., Fernando, L., Fernández, J. F., Eds.; Springer: New York, 2014; pp 191–220.

(7) Coulon, C.; Miyasaka, H.; Clérac, R. *Struct. Bonding (Berlin)* **2006**, *122*, 163–206.

(8) (a) Ishikawa, R.; Katoh, K.; Breedlove, B. K.; Yamashita, M. *Inorg. Chem.* **2012**, *51*, 9123–9131. (b) Bhargavi, G.; Rajasekharan, M. V.; Costes, J.-P.; Tuchagues, J.-P. *Dalton Trans.* **2013**, *42*, 8113–8123. (c) Senapati, T.; Pichon, C.; Ababei, R.; Mathoniere, C.; Clérac, R. *Inorg. Chem.* **2012**, *51*, 3796–3812. (d) Boeckmann, J.; Wriedt, M.; Naether, C. *Chem.—Eur. J.* **2012**, *18*, 5284–5289. (e) Zhang, W.-X.; Shiga, T.; Miyasaka, H.; Yamashita, M. *J. Am. Chem. Soc.* **2012**, *134*, 6908–6911. (g) Sahoo, S.; Sutter, J.-P.; Ramasesha, S. *J. Stat. Phys.* **2012**, *147*, 181–193. (h) Liu, R. N.; Hu, P.; Li, L. C.; Liao, D. Z.; Sutter, J.-P. *Sci. China Chem.* **2012**, *55*, 997–1003. (j) Li, Z.-X.; Jie, W.; Zha, G.; Wang, T.; Xu, Y. *Eur. J. Inorg. Chem.* **2012**, *22*, 3537–3540. (k) Liu, R.; Xiong, C.; Zhao, S.; Wu, J.; Li, Q.; Fang, D. *Inorg. Chem. Commun.* **2012**, *22*, 104–107. (l) Tomkowicz, Z.; Rams, M.; Balanda, M.; Foro, S.; Nojiri, H.; Krupskaya, Y.; Kataev, V.; Buchner, B.; Nayak, S. K.; Yakhmi, J. V.; Haase, W. *Inorg. Chem.* **2012**, *51*, 9983–9994. (m) Hoshino, N.; Iijima, F.; Newton, G. N.; Yoshida, N.; Shiga, T.; Nojiri, H.; Nakao, A.; Kumai, R.; Murakami, Y.; Oshio, H. *Nat. Chem.* **2012**, *4*, 921–926. (n) Visinescu, D.; Jeon, I.-R.; Madalan, A. M.; Alexandru, M.-G.; Jurca, B.; Mathoniere, C.; Clérac, R.; Andruh, M. *Dalton Trans.* **2012**, *41*, 13578–13581. (o) Yao, M.-X.; Zheng, Q.; Qian, K.; Song, Y.; Gao, S.; Zuo, J.-L. *Chem.—Eur. J.* **2013**, *19*, 294–303. (p) Mougel, V.; Chatelain, L.; Hermle, J.; Caciuffo, R.; Colineau, E.; Tuna, F.; Magnani, N.; Degeyer, A.; Pécaut, J.; Mazzanti, M. *Angew. Chem. Int.* **2014**, *53*, 819–823. (q) Vaz, M. G. F.; Cassaro, R. A. A.; Akpinar, H.; Schlueter, J. A.; Lahti, P. M.; Novak, M. A. *Chem.—Eur. J.* **2014**, DOI: 10.1002/chem.201304852.

(9) Glauber, R. *J. Math. Phys.* **1963**, *4*, 294.

(10) Coulon, C.; Clérac, R.; Lecren, L.; Wernsdorfer, W.; Miyasaka, H. *Phys. Rev. B* **2004**, *69*, 132408.

(11) (a) Miyasaka, H.; Saitoh, A.; Abe, S. *Coord. Chem. Rev.* **2007**, *251*, 2622–2664. (b) Sun, H.-L.; Wang, Z.-M.; Gao, S. *Coord. Chem. Rev.* **2010**, *254*, 1081–2791. (c) Wang, X.-Y.; Avendaño, C.; Dunbar, K. R. *Chem. Soc. Rev.* **2011**, *40*, 3213–3238. (d) Yoon, J. H.; Lee, J. W.; Ryu, D. W.; Choi, S. Y.; Yoon, S. W.; Suh, B. J.; Koh, E. K.; Kim, H. C.; Hong, C. S. *Inorg. Chem.* **2011**, *50*, 11306–1308. (e) Dreiser, J.; Pedersen, K. S.; Schnegg, A.; Holldack, K.; Nehrkorn, J.; Sigrist, M.; Tregenna-Piggott, P.; Mutka, H.; Weihe, H.; Mironov, V. S.; Bendix, J.; Waldmann, O. *Chem.—Eur. J.* **2013**, *19*, 3693–3701. (f) Qian, K.; Huang, X.-C.; Zhou, C.; You, X.-Z.; Wang, X.-Y.; Dunbar, K. R. *J. Am. Chem. Soc.* **2013**, *135*, 13302–13305. (g) Miyasaka, H.; Saitoh, A.; Yamashita, M.; Clérac, R. *Dalton Trans.* **2008**, 2422–2427.

(12) (a) Feng, X. W.; Liu, J.; Harris, T. D.; Hill, S.; Long, J. R. *J. Am. Chem. Soc.* **2012**, *134*, 7521–7529. (b) Li, Y.-H.; He, W.-R.; Ding, X.-H.; Wang, S.; Cui, L.-F.; Huang, W. *Coord. Chem. Rev.* **2012**, *256*, 2795–2815. (c) Toma, L. M.; Pasan, J.; Catalina, R.-P.; Julve, M.; Lloret, F. *Dalton Trans.* **2012**, *41*, 13716–13726. (d) Kang, S.; Kanegawa, S.; Sato, O. *Dalton Trans.* **2012**, *41*, 13575–13577. (e) Dong, D.-P.; Liu, T.; Zheng, H.; Zhao, L.; Zhuang, P.-F.; He, C.; Duan, C.-Y. *Inorg. Chem., Commun.* **2012**, *24*, 153–156. (f) Chorazy, S.; Nakabayashi, K.; Imoto, K.; Mlynarski, J.; Sieklucka, B.; Ohkoshi, S. *J. Am. Chem. Soc.* **2012**, *134*, 16151–16154. (g) Toma, L. M.; Ruiz-Perez, C.; Pasan, J.; Wernsdorfer, W.; Lloret, F.; Julve, M. *J. Am. Chem. Soc.* **2012**, *134*, 15265–15268. (h) Bhowmick, I.; Hillard, E. A.; Dechambenoit, P.; Coulon, C.; Harris, T. D.; Clérac, R. *Chem. Commun.* **2012**, *48*, 9717–9719.

(13) (a) Choi, H. J.; Sokol, J. J.; Long, J. R. *Inorg. Chem.* **2004**, *43*, 1606–1608. (b) Miyasaka, H.; Takahashi, H.; Madanbashi, T.; Sugiura, K.; Clérac, R.; Nojiri, H. *Inorg. Chem.* **2005**, *44*, 5969–5971. (c) Tregenna-Piggott, P. L. W.; Sheptyakov, D.; Keller, L.; Klokishner, S. I.; Ostrovsky, S. M.; Palii, A. V.; Reu, O. S.; Bendix, J.; Brock-Nannestad, T.; Pedersen, K.; Weihe, H.; Mutka, H. *Inorg. Chem.* **2009**, *48*, 128–134. (d) Kara, H.; Azizoglu, A.; Karaoglu, A.; Yahsi, Y.; Gungor, E.; Caneschi, A.; Sorace, L. *CrystEngComm* **2012**, *14*, 7320–7329.

(14) Ferbinteanu, M.; Miyasaka, H.; Wernsdorfer, W.; Nakata, K.; Sugiura, K.; Yamashita, M.; Coulon, C.; Clérac, R. *J. Am. Chem. Soc.* **2005**, *127*, 3090–3099.

(15) Miyasaka, H.; Madanbashi, T.; Saitoh, A.; Motokawa, N.; Ishikawa, R.; Yamashita, M.; Bahr, S.; Wernsdorfer, W.; Clérac, R. *Chem.—Eur. J.* **2012**, *18*, 3942–3954.

(16) Re, N.; Gallo, E.; Floriani, C.; Miyasaka, H.; Matsumoto, N. *Inorg. Chem.* **1996**, *35*, 6004–6008.

(17) McCarthy, P. J.; Hovey, R. J.; Ueno, K.; Martell, A. E. *J. Am. Chem. Soc.* **1955**, *77*, 5820–5824.

(18) (a) Boucher, L. J.; Day, V. W. *Inorg. Chem.* **1977**, *16*, 1360–1367. (b) Wernsdorfer, W. *Adv. Chem. Phys.* **2001**, *118*, 99.

(19) Bruker, SHELXTL, version 6.22; Bruker AXS Inc.: Madison, WI, 2003.
(20) Sheldrick, G. M. SADABS, Program for empirical X-ray absorption correction, Bruker-Nonius, 1990.
(21) Computer sofware: Apex2 V.1.27 (Bruker, 2005), *SHELXS97* (Sheldrick, 1990), *SHELXL97* (Sheldrick, 1997), *SHELXTL* V6.22 (Bruker, 2000−2005), local programs.
(22) Blatov, V. A. *Compcomm Newslett.* **2006**, *7*, 4−38.
(23) Atanasov, M.; Comba, P.; Daul, C. A.; Hauser, A. *J. Phys. Chem. A* **2007**, *111*, 9145−9163.
(24) Peresypkina, E. V.; Vostrikova, K. E. *Dalton Trans.* **2012**, *41*, 4100−4106.
(25) Miyasaka, H.; Okawa, H.; Miyazaki, A.; Enoki, T. *Inorg. Chem.* **1998**, *37*, 4878−4883.
(26) O'Keeffe, M.; Andersson, S. *Acta Crystallogr.* **1977**, *A33*, 914−923.
(27) Seiden, J. *J. Phys., Lett.* **1983**, *44*, 947.
(28) Mydosh, J. A. *Spin Glasses: An Experimental Introduction*; Taylor and Francis: London, 1993; p 67.
(29) Cole, K. S.; Cole, R. H. *J. Chem. Phys.* **1941**, *9*, 341−351.
(30) Luscombe, J. H.; Luban, M.; Reynolds, J. P. *Phys. Rev. E* **1996**, *53*, 5852−5860.
(31) Wernsdorfer, W.; Orozco, E.; Hasselbach, K.; Benoit, A.; Barbara, B.; Demoncy, N.; Loiseau, A.; Pascard, H.; Mailly, D. *Phys. Rev. Lett.* **1997**, *78*, 1791.
(32) Ni, Z. H.; Tao, J.; Wernsdorfer, W.; Cuiand, A. L.; Kou, H. Z. *Dalton Trans.* **2009**, 2788−2794.
(33) Reddy, K. R.; Rajasekharan, M. V.; Tuchagues, J.-P. *Inorg. Chem.* **1998**, *37*, 5978.
(34) (a) Miyasaka, H.; Matsumoto, N.; Okawa, H.; Re, N.; Gallo, E.; Floriani, C. *J. Am. Chem. Soc.* **1996**, *118*, 981−994. (b) Ni, W. W.; Ni, Z. H.; Cui, A. L.; Liang, X.; Kou, H. Z. *Inorg. Chem.* **2007**, *46*, 22−33.
(35) Peresypkina, E. V.; Majcher, A. M.; Rams, M.; Vostrikova, K. E. *Chem. Commun.* **2014**, *50*, 7150−7153.